Journal of Biomechanics 82 (2019) 251–258

Contents lists available at ScienceDirect

Journal of Biomechanics

journal homepage: www.elsevier.com/locate/jbiomech
www.JBiomech.com

Effects of seating load magnitude and load orientation on seating mechanics in 5°40′ mixed-alloy modular taper junctions

David Pierre [a,b], Viswanathan Swaminathan [c], Laura Scholl [c], Kevor TenHuisen [c], Jeremy L. Gilbert [a,b,*]

[a] Syracuse University, Syracuse Biomaterials Institute, Syracuse, NY, United States
[b] Department of Bioengineering, Clemson University, Charleston, SC, United States
[c] Stryker, Mahwah, NJ, United States

ARTICLE INFO

Article history:
Accepted 29 October 2018

Keywords:
Seating mechanics
Assembly load
Assembly orientation
Orthopedic implants
Mechanically assisted crevice corrosion
Taper stability

ABSTRACT

Background: Mechanically-assisted crevice corrosion of modular tapers continues to be a concern in total joint replacements. Surgical factors that may affect taper seating mechanics include seating load magnitude and load orientation. Seating mechanics is defined as the seating load versus displacement behavior. In this study, mixed-alloy (CoCrMo/Ti-6Al-4V) modular head-neck 5°40′ taper junctions were seated over a range of axially-oriented loads and off-axis orientations, capturing load-displacement during seating. The goals of the study were to assess the effects of seating load magnitude and load orientation on seating mechanics and correlate those findings with the taper pull-off load.

Methods: A testing fixture measured head-neck seating displacement as the load was quasistatically applied. Motion was captured using two non-contact differential variable reluctance transducers which were mounted to the neck targeting the head. Seating experiments ranged from 1000 N to 8000 N. Load orientation ranged from 0° to 20° at 4000 N.

Results: Seating load-displacement behavior at different seating loads showed a consistent characteristic behavior. Testing demonstrated increased seating displacement with seating load. Pull-off loads increased with seating load and were approximately 44% of the seating load across the range of seating loads investigated. Seating load orientation up to 20° had no significant effect on seating displacement and taper pull-off load.

Conclusion: Increased seating load magnitude increased seating displacement, work of seating and pull-off loads in mixed-alloy 5°40′ head-neck tapers. Altering load orientation up to 20° off-axis had no significant effect. Direct measurements of seating mechanics provides insights into the locking of taper junctions.

© 2018 Elsevier Ltd. All rights reserved.

1. Introduction

Modular tapers in total joint replacements became widely available in the mid-to-late 1980s. Modularity allows for different material combinations, component size variations and ease of revision surgery compared to previous monoblock components (McCarthy et al., 1997). Ideally, modularity optimizes implant performance and allows for intraoperative flexibility. The benefits of modularity have extended beyond patients and hospitals. Manufacturers were able to reduce inventory and cost of storage per implant which decreased the financial burden on the healthcare system (Barrack, 1994; Cameron, 1996; Hozack and Mesa, 1996).

However, modular tapers have shown instances of mechanically assisted crevice corrosion (MACC) (Gilbert, 2006). MACC is the result of mechanical loading and cyclic motion at the taper interface producing fretting corrosion debris (ions and oxide particles) which can be distributed locally and systemically (Gilbert et al., 1993; Gilbert, 2006; Gilbert, 2011; Gilbert and Jacobs, 1997; Goldberg et al., 1997; Jacobs et al., 1995). Significant levels of corrosion have been seen in a variety of taper junctions and implant designs, and recent clinical studies have reported an increase in corrosion–associated adverse local tissue reactions, which may lead to implant failure and the need for revision (Langton, 2010; Cooper et al., 2012; Cooper et al., 2013; Cooper, 2014).

The influence of seating load magnitude on taper mechanics has been studied. These studies have suggested that an increase in assembly load between the femoral components increased taper stability and reduced motion between the interface during loading

* Corresponding author at: Clemson University – Medical University of South Carolina, Program in Bioengineering, 68 President Street, Rm BEB101D, MSC 501, Charleston, SC 29425, United States.
E-mail address: jlgilbe@clemson.edu (J.L. Gilbert).

https://doi.org/10.1016/j.jbiomech.2018.10.037
0021-9290/© 2018 Elsevier Ltd. All rights reserved.

(Jauch et al., 2011; Rehmer et al., 2012). Few of these studies, however, have incorporated a controlled seating methodology able to measure the seating mechanics (load-displacement behavior) during assembly (Ouellette et al., 2017). In addition, there are few if any studies known to the authors that have directly assessed the variability in surgical practice (particularly load orientation) and correlated the effect on taper locking and pull-off strength.

Hence, in this study, mixed-alloy modular 5°40′ taper junctions were assembled over a range of seating loads and loading orientations. Throughout loading, the seating load-displacement behavior was captured. The goals of this study were to assess the effects of load magnitude and orientation on seating load-displacement mechanics and to correlate these to the pull-off load. It is hypothesized that an increase in seating load magnitude and decrease in the load-neck orientation angle will improve seating displacement and taper pull-off loads.

2. Materials and Methods

2.1. Specimen design

Test samples consisted of Ti-6Al-4V trunnions and CoCrMo heads with nominal taper angles of 5°40′ (provided by Stryker, see line drawing in Fig. 1a). Trunnion samples were machined to a cylindrical geometry with the neck and taper region on one end. The trunnion taper dimensions were a nominal engagement length of 11 mm, an apical diameter (most proximal taper region) of 12 mm. The trunnion taper surface was a ground finish as they would for commercial use, with no spiral thread or other topography. The heads were commercially manufactured CoCrMo alloy with a 36 mm diameter and a + 5 mm head offset. The female taper surface topography was as-ground. The nominal taper angles for both head and neck were nominally 5° 40′′ (5.667°), with a measured angle ranging between 5.627 and 5.646°for the trunnion and 5.694 to 5.712°for the head tapers. The head and trunnion tapers were matched to provide a consistent angular mismatch of 0.066 to 0.68° (with the head slightly larger in angle than the trunnion for all cases).

For seating load magnitude testing, samples were axially seated at four load levels (n = 5): 1000, 2000, 4000 and 8000 N. For seating load orientation testing, three load orientation groups (n = 5) were seated to 4000 N at 0°, 10° and 20° orientation between the neck axis and the loading axis. A coordinate measurement machine (Wenzel LH87, Wenzel America) was used to measure the taper angles of the femoral head and trunnion prior to testing. The angle measurements were then used to pair the head and trunnion samples to minimize mismatch variation between sample pairs. Trunnion tapers were also characterized for surface roughness using White Light Interferometer (Zygo NewView 6000, Zygo) to confirm the surface finish. Both head and trunnion surfaces were as ground as for commercial use with no imparted ridges or spiral threads. The surface roughnesses obtained were in the range of 0.18 μm (SD = 0.012 μm, n = 20) for the Ra value.

2.2. Specimen mounting and displacement measurement system

Samples were positioned directly under the load applicator. Off-axis samples were mounted in an angled fixture and held fixed with an aluminum screw which allowed the load to be applied at the predetermined angles of 10° and 20° (Fig. 1b). Seating displacements were captured using two non-contact eddy current sensors with a range of 1 mm (2 μm resolution) mounted to the superior and inferior portions of the stem (Micro-Epsilon™, Raleigh, NC). Sensors targeted aluminum plates fixed to the head. Displacement and load were captured by a custom made data acquisition and instrument control program (LabView™) at a rate of 100 points/s.

2.3. Test protocol

Before testing, male and female taper junctions were cleaned with ethanol to remove contaminants from the surfaces. The heads of each sample were placed manually on the neck and axially preloaded to 50 N. Samples were then tested to the predetermined seating load magnitude and orientation specifications. Loads were applied with a servohydraulic test frame at a rate of 200 N/s and held at the peak load for 5 s before unloading (Instron). Post seating, tensile on-axis pull-off loads were applied using a test fixture with a fork-like opening that supported the head just outside of the taper junction and the trunnion sample was mounted to a chain using the bolt hole in the base of the trunnion to apply an axial ten-

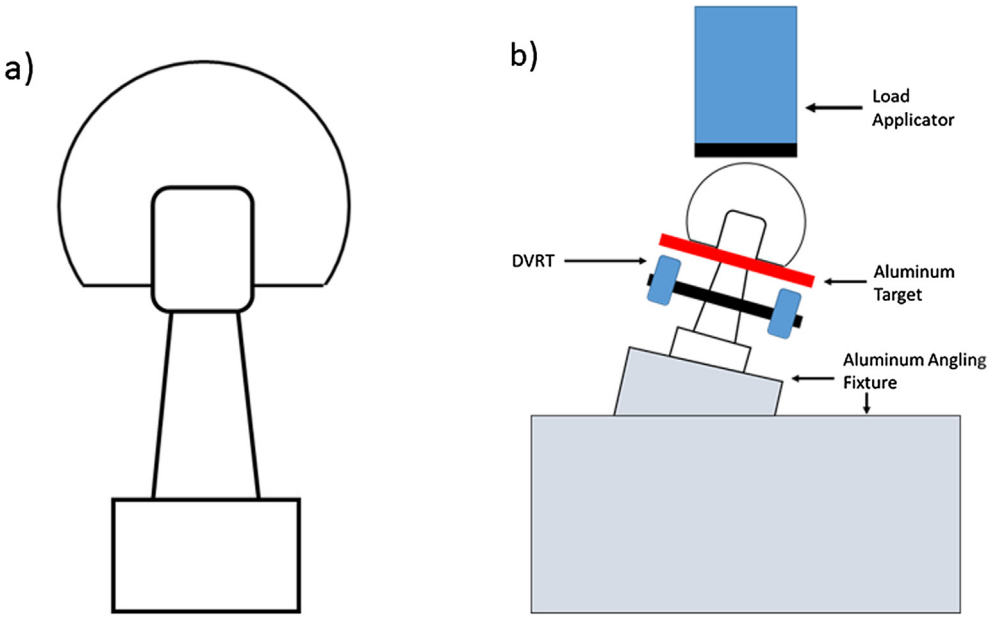

Fig. 1. (a) Line drawing of Ti-6Al-4V trunnions and CoCrMo heads with nominal taper angles of 5°40′. (b) Aluminum fixture which securely holds couponed trunnion with DVRTs fixed to the superior and inferior portions of the stem targeting the head under the load applicator.

sile load to the junction with a displacement rate of 5 mm/min (MTS858, MTS Systems Corporation, Minnesota) until the taper interlock was overcome.

2.4. Data analysis

Acquired displacement data was used to determine the seating displacement by taking the position at 50 N preload to maximum loading and then unloading in order to effectively compare sample groups. A one-way ANOVA test with post-hoc Tukey analysis was used to determine differences, with a significance level of 0.05.

The seating displacement was determined as the difference between the rigid final displacement, (i.e., the displacement recorded after complete unloading), and the rigid initial displacement, (i.e., the displacement recorded at 50 N of initial seating load). Final displacements were taken at unload to remove the elastic deformation of the system from the measurement, while the 50 N initial load was used to assure an initial seating location was consistently defined.

For the off-axis orientation of seating, significant elastic bending displacements were superimposed on the rigid body seating motion. The greater the off-axis alignment, the more bending displacements were present. To accommodate these elastic-based bending displacements, a method was used to correct the seating plots for the elastic displacements. This was accomplished by taking the instantaneous load and dividing it by the slope of the unloading portion of the seating tests at each point in time. This results in a measure of the elastic-based displacements which are then subtracted from the total measured displacements to obtain the corrected rigid-body motion. This correction was applied prior to determining the work of seating and the seating displacements, however, the results obtained from both are not affected by these elastic motions as they are fully recovered after unloading (Mali and Gilbert, 2016; Pierre and Gilbert, 2016; Pierre and Gilbert, 2014).

The work of seating was calculated using the Trapezoidal Rule to determine the area under the curve for seating load-displacement graphs:

$$W = \sum_{i=0}^{n} \left(\frac{F_{i+1} + F_i}{2} \right) * (D_{i+1} - D_i)$$

F is the load applied, i is the indicial point (which is summed over n points covering the complete load-unload cycle) and D is displacement. The work of seating represents the energy required to create the taper locking.

3. Results

3.1. Load magnitude analysis: Seating displacement

Fig. 2a illustrates an example of the load and displacement versus time relationship during a seating test. The displacement increased with the load overtime until the peak load was reached (4000 N in this case) and held for 5 s before unloading. The maximum displacement was achieved at maximum load and upon unloading the sample experienced an elastic rebound before settling at its final displacement.

Seating load-displacement behavior at the various seating loads showed a consistent characteristic behavior. During seating (Fig. 2a), displacements rose non-linearly until reaching the peak load. The unloading behavior, from maximum load to zero load reflects the recovery of the elastic energy of the system.

The corresponding load-displacement plots from several different seating experiments to different maximum loads are shown in Fig. 2b. The loading portion of these plots rises parabolically with displacement to the maximum load and then unloads in a linear load-displacement fashion indicating elastic unloading behavior. The area inside the curves is the total work of seating and is comprised of both elastic and frictional interactions which is, in part, why the loading portion is parabolic.

It is interesting to note that the shape of the seating curves overlay one another from 1000 to 8000 N indicating a consistent and reproducible seating behavior for these tapers. In each loading scenario, the unloading portion of the plots appear to be parallel indicating that the elastic rebound during unloading is consistent between samples as well. The y-intercept of the unloading curves reflects the final seating displacement (Fig. 2b).

3.2. Load magnitude results

3.2.1. Seating displacement

The average final seating displacement for the superior and inferior sensors show a power-law increase which is close to a square-root dependence (see regression lines, Fig. 3) in seating displacement with an increase in seating load magnitude, which is consistent with the parabolic dependence in Fig. 2b. Each group was statistically significantly different (Fig. 3) ($p < 0.05$).

3.2.2. Work of seating

The average work of seating values also demonstrated a statistically significant parabolic increase with an increase in seating

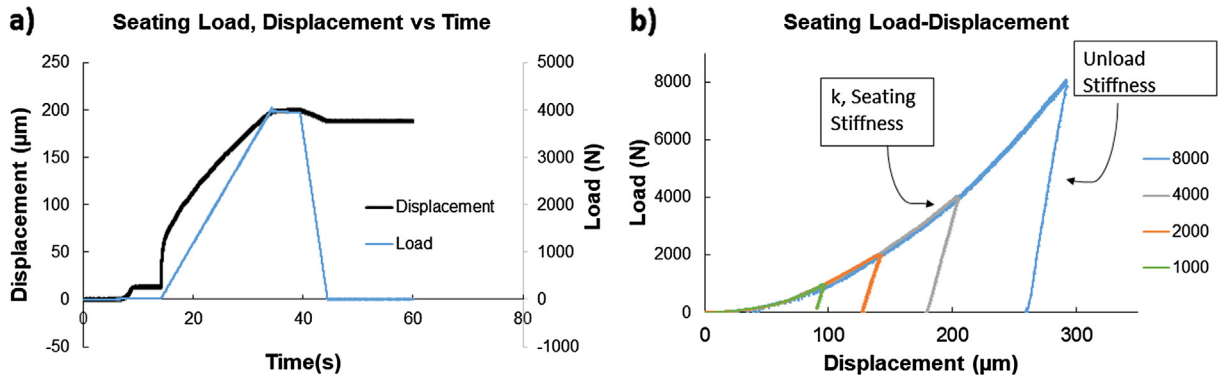

Fig. 2. (a) An example of one seating test result with superimposed seating load vs. time and displacement vs. time plots loaded to 4000 N. This illustrates the taper motion during loading and unloading. (b) Superimposed seating load-displacement plots for the different load magnitude groups. The graph highlights the characteristic behavior of the taper during seating and unloading. The plots for different maximum load levels are superimposed with similar unloading slopes.

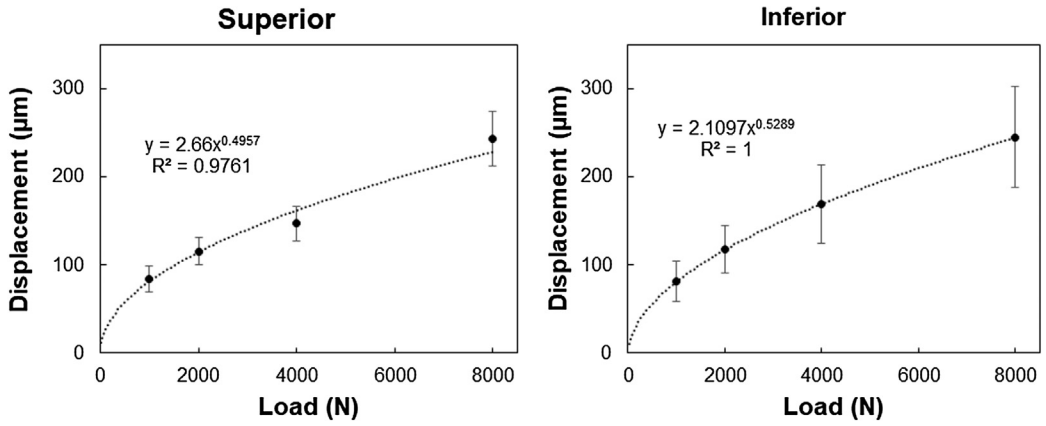

Fig. 3. Average seating displacement vs. load demonstrates a power-law increase. Each load magnitude group was statistically significantly different ($p < 0.05$).

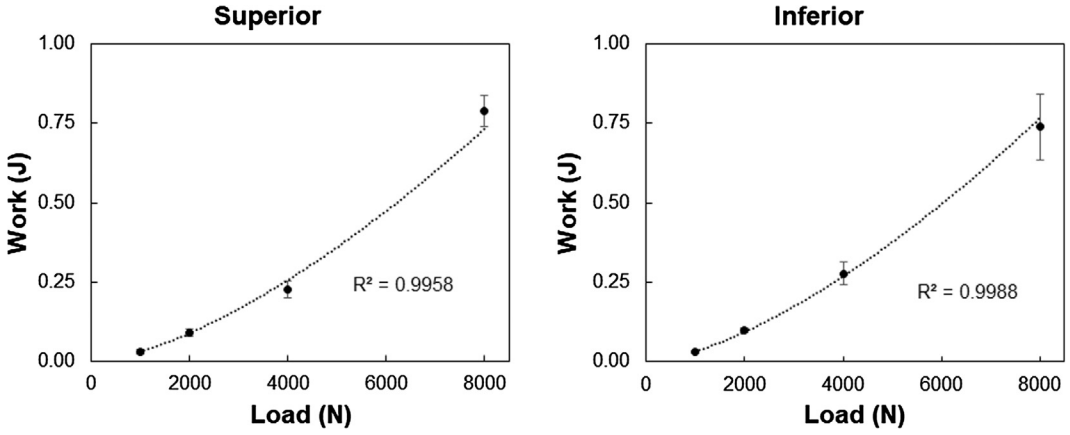

Fig. 4. Average work of seating vs. load shows parabolic increase in work of seating with increase in load magnitude. Each load magnitude group was statistically significantly different from one another ($p < 0.05$).

load magnitude for both sensors (Fig. 4, $p < 0.05$). The average work of seating was approximately 0.2 to 0.25 J at 4000 N seating load.

3.2.3. Pull-off load

Pull-off loads for similar tapers typically reflect the seating load magnitude, requiring about 48% of the seating load magnitude to be distracted (Mali and Gilbert, 2016; Ouellette et al., 2017; Pierre et al., 2018). The results of testing showed the pull-off loads increased linearly with an increase in seating load; all groups were significantly different (Fig. 5, $p < 0.05$).

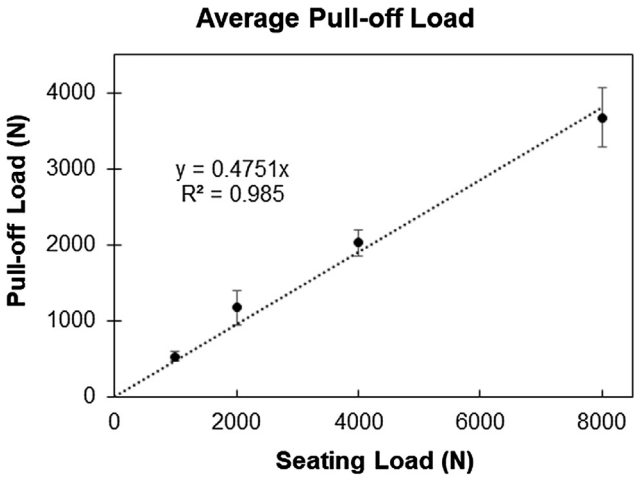

Fig. 5. Average pull-off load for range of loads. Each group was statistically significantly different ($p < 0.05$). The pull-off load was approximately 48% of the seating load.

3.3. Load orientation results:

3.3.1. Seating displacement

Seating displacement of off-axis samples was comprised of both rigid motion as well as elastic motion (associated with the compression and bending of the component in conjunction with such load orientations).

With an increased angle in the seating load orientation, the bending of the neck and elastic motion also increased. Fig. 6 illustrates the trend in elastic bending in the seating load-displacement data. As the seating load orientation increased from 0° to 10° to 20°, an increase in the bending-based displacements is observed with the superior sensor seeing tensile-based displacement (opposite of the seating motion), while the inferior sensor senses compression-based displacement (additive to the seating motion). As the off-axis orientation increased, more bending deformation was present in the displacement measurements. The superior sensor reported elastic-bending displacements that were opposite of the seating direction, while the elastic bending displacements inferiorly were in the same direction as the seating displacements. The unloading portions of these curves represent elastic unloading of

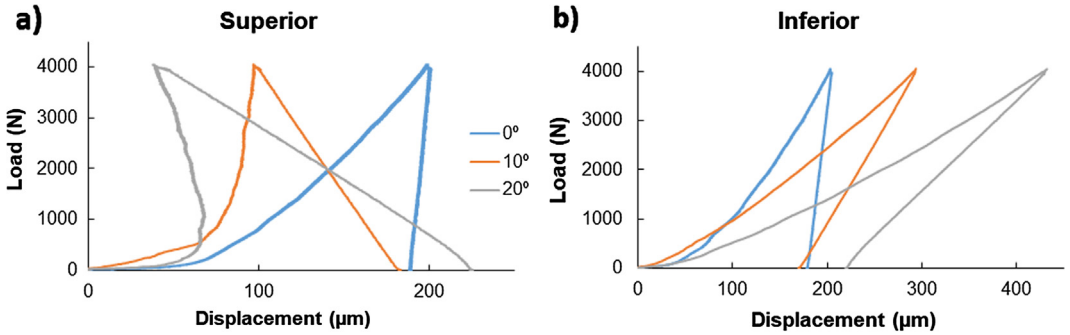

Fig. 6. Load vs. displacement graphs for three different load orientation groups. (a) Superior sensor load-displacement behavior and (b) inferior sensor behavior. These data show the elastic bending nature of off-axis load samples compared to axially loaded samples. Increasing the orientation angle increased the elastic displacement captured by the sensors.

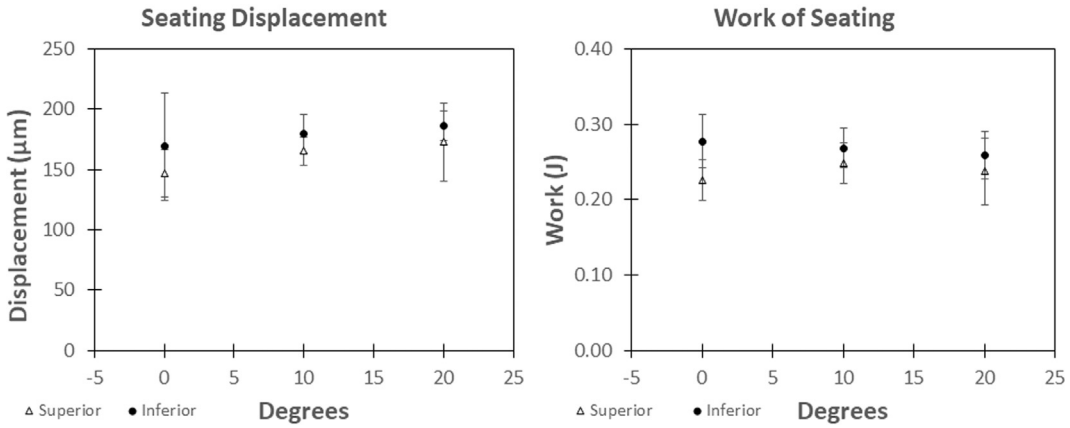

Fig. 7. Average a) seating displacement and b) work of seating per group as a function of seating orientation (0 to 20°at 4000 N). No statistically significant differences were observed between the groups. Average seating displacement was approximately 150 to 200 µm. Average work of seating was approximately 0.2 to 0.3 J for a 4000 N seating load.

the sample only and depend on the sample geometry, material, and the location of the sensor and target.

The results of seating displacement testing showed, despite the increase in load orientation, there was no statistical difference in average seating displacement between orientation groups, with an average displacement of 150–190 µm (Fig. 7a).

3.3.2. Work of seating

There was no statistically significant difference in work of seating (Fig. 7b) for the different orientations at 4000 N in this test.

3.3.3. Pull-off load

The pull-off loads for the different orientation groups (Fig. 8) showed no statistically significant differences. The average pull-off load was approximately 2000 N, 50% of the seating load magnitude for these tests.

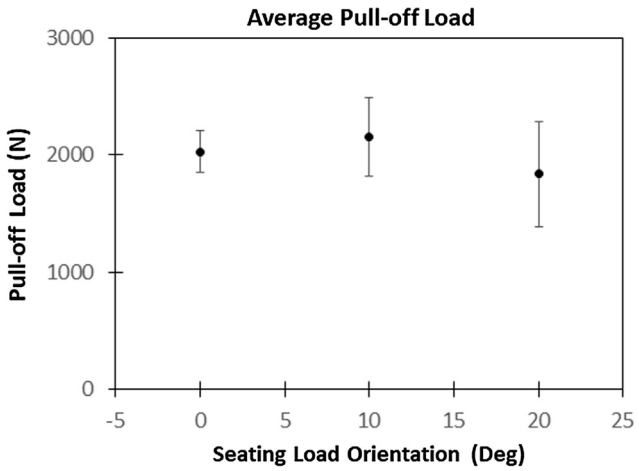

Fig. 8. Average pull-off load of 0°, 10° and 20° orientation groups. Groups were not statistically different with an average pull-off load of 2000 N.

4. Discussion

Seating load magnitude and load orientation effects on seating mechanics and taper locking stability were quantitatively studied in an effort to simulate possible variations in orientation that may arise during surgical assembly. Under the conditions in this study, seating load magnitude had a direct effect on seating displacement, work of seating and taper pull-off. However, increasing the seating load orientation up to 20° had no significant effect on seating mechanics or taper pull-off.

4.1. Seating load-displacement plot analysis

The characteristic load–displacement behavior for both loading and unloading of the 5°40′ CoCrMo/Ti6Al4V tapers (Fig. 2b) has a number of important parameters and concepts associated with it that deserve further consideration.

These include the loading behavior, the unloading behavior and the work of seating. To understand each of these elements, the 4000 N load-displacement plot from Fig. 2b is reproduced in Fig. 9 along with addition plots based on the discussion below.

The loading behavior for axially loaded tapers, as noted experimentally, was parabolic in nature. That is, it can be represented by

$$F = k\delta^2 \text{ (for loading)} \quad (1)$$

where δ is the seating displacement, F is the seating load and k is the seating stiffness parameter which can be found from inputting F and δ at a specific load. For these specific tapers, k = 1x10^5 N/mm^2 and the plot of this function is overlaid on Fig. 9 for clarity and shows complete overlap with the measured results.

This behavior consists of both the elastic compression strain energy developed with continued pushing of the trunnion into the taper and the frictional work dissipated across the surfaces. The seating stiffness parameter, k, is also dependent on a number of design and material factors that include the taper macroscopic geometry (diameter, engagement length), microscopic geometry (roughness), material moduli, interfacial coefficient of friction and taper half-angle (Gilbert et al., 2015) and the sensor configuration. This latter parameter (sensor configuration) affects the total distance between the sensor mounting point and the aluminum target mounting point. The larger this distance, the larger the elastic displacements measured. When bending is involved, then the distance of the sensor from the neutral axis of bending is important as well.

For unloading, the taper is locked and no rigid body motion occurs between the two surfaces (assuming the coefficient of friction is high enough to stick the interfaces) and the load-displacement plots during unloading are linear with an unloading slope (k_2). This parameter depends on the sensor configuration, sample geometry, moduli and loading orientation. For axial loading, k_2 reflects an elastic compressive unloading, while the off-axis unloading reflects both compressive and bending derived elastic displacements. It should be noted (see Fig. 6), that the elastic displacements sensed by the sensor during the off axis seating experiments show clear signs of elastic bending based displacements. The greater the off-axis loading the larger were the elastic bending based displacements noted. These displacements reached up to 200 mm in the 20° seating experiments and are well above any potential rigid-body based micromotion that may be present at the taper during the unloading. Even in the axially loaded samples, the unloading elastic displacements observed were linear and about 30 to 50 mm which is larger than the typical micromotion reported and therefore is likely related to the compressive elastic displacements of the trunnion. The average inferior displacements (see Fig. 7a) were always slightly larger than the superior displacements indicating a tilting like motion of the head on the trunnion as seating progress, however, the differences in seating between sensors was not statistically significant.

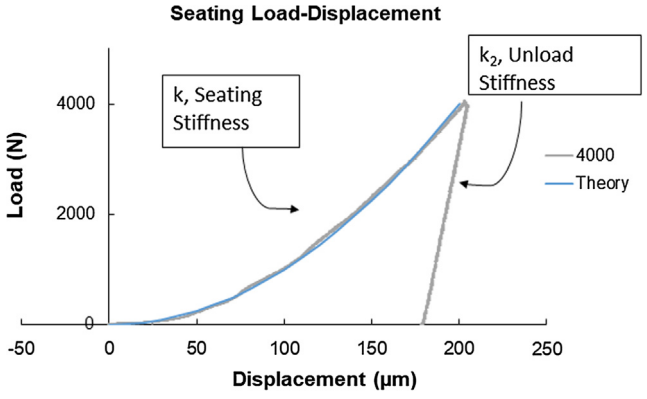

Fig. 9. A single seating load displacement plot for a taper seated to 4000 N. Also shown is the fitted curve (Eq. (1)), and the fitting parameters for loading (k) and unloading (k_2). Note the excellent fit of the parabolic function to the seating curve. The area inside the loading and unloading curves represents the frictional energy dissipated in seating, while the area under the elastic unloading portion represents the recoverable elastic energy. The area under the loading curve is comprised of both friction and elastic energy.

4.1.1. Work of seating

The work of seating is the work done during loading minus the work done during unloading. These work terms are the area under the seating load-displacement plots (Fig. 9). The area under the loading curve can be analyzed from the following. Using a free body diagram of the seating force (see Fig. 10) it can be seen that there are interfacial pressures, P and frictional stresses, τ, developed at the interface according to:

$$F = (P\sin\alpha + \tau\cos\alpha)A = PA(\sin\alpha + \mu\cos\alpha) \quad (2)$$

where F is the seating force, P is the nominal contact pressure, A is the nominal contact area and μ is the coefficient of friction (where the frictional stress, τ = μP), and α is the taper half angle.

The work of seating (during loading) is simply:

$$W = \int_0^{\delta_{max}} F \cdot d\delta = \int_0^{\delta_{max}} k\delta^2 \cdot d\delta = k\frac{\delta_{max}^3}{3} \quad (3)$$

While the work of elastic unloading (i.e., the elastic energy released on unloading) is

$$W_{elastic} = \int_{\delta_f}^{\delta_{max}} F \cdot d\delta = \int_{\delta_f}^{\delta_{max}} k_2(\delta - \delta_f) \cdot d\delta$$
$$= k_2\left[\frac{\left(\delta_{max}^2 - \delta_f^2\right)}{2} - \delta_f(\delta_{max} - \delta_f)\right] \quad (4)$$

The net work of seating is the difference between these two energies

$$W_{seating} = W - W_{elastic}$$
$$= k\frac{\delta_{max}^3}{3} - k_2\left[\frac{\left(\delta_{max}^2 - \delta_f^2\right)}{2} - \delta_f(\delta_{max} - \delta_f)\right] \quad (5)$$

Alternatively, the seating work can be analyzed using Eq. (2) and (3) as:

$$W = \int_0^{\delta_{max}} F \cdot d\delta = \int_0^{\delta_{max}} PA(\sin\alpha + \mu\cos\alpha) \cdot d\delta \quad (6)$$

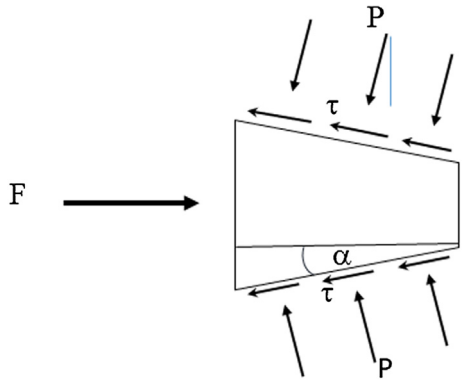

Fig. 10. Free body diagram for a taper under external force F. Reactive pressure, P and frictional shear stress, τ, act to balance the instantaneous applied force, F. Taper half-angle, α, affects the components of pressure.

where the two terms reflect the elastic pressure (sine term) and friction (cosine term) contributions to the work. Eq. (6) can be combined with Eq. (1) and (2) to result in:

$$W = \int_0^{\delta_{max}} k\delta^2 \left(\frac{\sin\alpha}{\sin\alpha + \mu\cos\alpha} + \frac{\mu\cos\alpha}{\sin\alpha + \mu\cos\alpha} \right) \cdot d\delta \quad (7)$$

The two terms in Eq. (7) represent the fraction of the energy associated with the elastic-based pressure (first term) and the frictional energy (second term).

$$W = W_{elastic} + W_{friction} = k\frac{\delta_{max}^3}{3} \left(\frac{\sin\alpha}{\sin\alpha + \mu\cos\alpha} + \frac{\mu\cos\alpha}{\sin\alpha + \mu\cos\alpha} \right) \quad (8)$$

If one uses the appropriate values for α and μ (i.e., 2.83°, and 0.25 (Gilbert et al., 2015), respectively) about 16.5% of the work is elastic and 83.5% of the work is frictional or dissipated in seating.

For the plot in Fig. 9, based on numerical integrals of experimental data, the total work was 0.267 J, the elastic work was 0.044 J and the frictional work (or total net work in one seating load-unload cycle) was 0.223 J. From Fig. 9, the constant, k, is 100,000 N/mm^2, k_2 is 182,000 N/mm, δ_{max} = 200 μm, and δ_f is 178 μm. Using these values for the parameters shows essentially identical calculations for the total work, elastic work and frictional work as determined numerically (i.e., using Eqs. (3)–(5), respectively). In addition, the elastic and frictional work portions can be calculated using each term in Eq. (8) and again, the results are identical to that calculated directly from the experimental results. This shows the partitioning of elastic and frictional work depends on the taper angle and frictional interaction of the taper.

4.1.2. Pull-off load

Pull-off load testing, a standard taper stability assessment method, also showed a linear increase with seating load with a y-intercept which goes through 0 (Fig. 5). Gilbert et al. describes a mathematical relationship between the initial seating load and the corresponding pull-off load where pull-off loads are approximately half the initial seating load depending on taper characteristics including taper angle and coefficient of friction (Mali and Gilbert, 2016).

The rate of seating displacement is greater in the early (low load) stages of seating and diminish with increasing load as can be seen by the increasing slope of the load-displacement curves with increasing seating load. The relationship between seating load magnitude and the corresponding displacement were previously discussed in studies by Pennock and Jauch et al. however in these studies the femoral head was seated manually or impacted and the seating load-displacement behavior was not captured (Pennock, 2002; Jauch et al., 2013).

Seating load orientation up to 20° had no significant effect on seating displacement, work of seating or pull-off load. While not tested in this work, the average pull-off loads with increased mis-orientation beyond 20° may show a greater decrease in pull-off load.

There were limitations to the study. Most importantly, the loads applied in this study were quasistatic, not dynamic. Impaction of heads may create vibrations (elastic rocking, twisting, etc.) that may affect the motion of the head on the neck. It is unlikely, however, that inertial effects are present. The distance traveled (ca. 100 um), even over the time of impaction would not result in sufficient kinetic energy to induce inertial effects of seating. Thus, while quasistatic loading is not clinically relevant, the details of the seating interaction obtained from these tests and their link to design, materials and loading conditions offers insights into taper locking and the effects of material and design on taper engagement mechanics. In addition, a recent study comparing quasistatic to impaction loading effects on the pull off force showed no significant difference in pull off strength (Scholl et al., 2018) for axial impaction. In another recent study using a 1D kinetic model of head-neck impaction, the time to seat a head onto a trunnion during impulses that spanned a range of values was within about 1 ms. It was observed in this model that the seating motion during impaction is completed prior to any significant vibrational motion that may subsequently arise (Gilbert et al., 2018).

Another limitation of the study is that the motion recorded during testing was only from two sensors diametrically opposed to one another. This configuration was able to capture rocking and pistoning but foregoes twisting and off-axis rocking during loading due to sensor placement. However, the symmetry of the seating orientation made any twisting motion to be unlikely and therefore pistoning and toggling motions (which can be captured with this configuration) are the principal motions present and the sensor orientation was able to capture this.

5. Conclusion

In conclusion, the seating load-displacement behavior of 5°40′ CoCrMo/Ti-6Al-4V head-neck tapers was directly measured using non-contact displacement sensors and quasistatic loading. The seating load magnitude had a direct correlation to seating displacement and pull-off load. The greater the seating load magnitude the greater the seating displacement, work of seating and pull-off load. Seating load-displacement data revealed a parabolic trend in seating as the load magnitude was increased, this information can be used to create an algorithm predicting seating displacement for an applied load when taper characteristics are known. The work of seating was shown to be comprised of friction work dissipated and elastic work which are a function of the taper angle and coefficient of friction.

The study also showed there was no significant effect of seating load orientation on seating displacement, work of seating and pull-off load when the seating load orientation was increased from 0° to 20°.

Seating load-displacement behavior is an important tool capable of assessing the materials, design and surgical factors that affect taper seating behavior.

Acknowledgements

Funding for this work was provided by Stryker Orthopedics Inc.

Conflict of Interest Statement

The author David Pierre has no current conflicts of interests. He has no financial or personal relationships, which may bias his work.

The authors Scholl, Swaminathan and TenHuisen are current employees with stock options at Stryker.

The corresponding author Jeremy L. Gilbert has royalties paid by Syracuse University. He is a paid consultant for DePuy Synthes, Zimmer Biomet, Medtronic, Stryker, Bayer, Omni LifeSciences, MiRus, TAV Medical, Woven Medical, Smith and Nephew and Pfizer. He has research support support from Stryker, NSF, ASHRE (American Society of Heating, Refrigeration, and Air Conditioning Engineers), Amedica, Incand Bausch and Lomb. Dr. Gilbert is Editor in Chief of the Journal of Biomedical Materials Research - Part B: Applied Biomaterials and serves on the council of the Society For Biomaterials.

References

Barrack, R.L., 1994. Modularity of prosthetic implants. J. Am. Acad. Orthop. Surg. 2 (1), 16–25.

Cameron, H.U., 1996. Modularity in primary total hip arthroplasty. J. Arthroplasty 11 (3), 332–334.

Cooper, H.J., Della Valle, C.J., Berger, R.A., Tetreault, M., Paprosky, W.G., Sporer, S.M., Jacobs, J.J., 2012. Corrosion at the head-neck taper as a cause for adverse local tissue reactions after total hip arthroplasty. J. Bone Joint Surg. 94 (18), 1655–1661.

Cooper, H.J., Urban, R.M., Wixson, R.L., Meneghini, R.M., Jacobs, J.J., 2013. Adverse local tissue reaction arising from corrosion at the femoral neck-body junction in a dual-taper stem with a cobalt-chromium modular neck. J. Bone Joint Surg. 95 (10), 865–872.

Cooper, H.J., 2014. The local effects of metal corrosion in total hip arthroplasty. Orthoped. Clin. North Am. 45 (1), 9–18.

Gilbert, J.L., Buckley, C.A., Jacobs, J.J., 1993. In-vivo corrosion of modular hip prosthesis components in mixed and similar metal combinations: the effect of crevice, stress, motion and alloy coupling. J. Biomed. Mater. Res. 27 (12), 1533–1544.

Gilbert, J.L., Jacobs, J.J., 1997. The Mechanical and Electrochemical Process Associated with Taper Fretting Crevice Corrosion: A Review. In: Marlowe, D. E., Parr, J.E., Mayor, M.B. (Eds.), Modularity of Orthopedic Implants, Amer Soc for Testing and Mat, Spec Tech Pub 1301. West Conshohockin, PA, pp. 45–59.

Gilbert, J.L., 2006. Mechanically Assisted Corrosion of Metallic Biomaterials. In: Cramer, S.D., Covino, B.S. (Eds.), ASM Handbook, 13C Corrosion: Environments and Industries. ASM International, Materials Park, OH, pp. 826–836.

Gilbert, J.L., 2011. Electrochemical Behaviour of Metals in the Biological Milieu. In: Ducheyne, P. (Ed.), Comprehensive Biomaterials. Elsevier, Amsterdam, Netherlands, pp. 21–48.

Gilbert, J.L., Mali, S.A., Sivan, S., 2015. Corrosion of Modular Tapers in Total Joint Replacements: A Critical Assessment of Design, Materials, Surfaces Structure, Mechanics, Electrochemistry and Biology. Amer Soc for Testing and Mat, Special Technical Publication on Implant Modularity, pp. 351–362.

Gilbert, J.L., Zhu, D., Smith, S., Pierre, D., 2018. A Model of Taper Seating Impaction: Head Size. Transactions of the Orthopedic Research Society, New Orleans, LA, Substrate Stiffness and Impulse Effects.

Goldberg, J.R., Buckley, C.A., Jacobs, J.J., Gilbert, J.L., 1997. Corrosion testing of modular hip implants. In: Marlowe, D.E., Parr, J.E., Mayor, M.B. (Eds.), Modularity of Orthopedic Implants, Amer Soc for Testing and Mat, Spec Tech Pub 1301. West Conshohockin, PA, pp. 157–174.

Hozack, W.J., Mesa, J.J., Rothman, R.H., 1996. Head-neck modularity for total hip arthroplasty: is it necessary? J. Arthroplasty 11 (4), 397–399.

Jacobs, J.J., Urban, R.M., Gilbert, J.L., Skipor, A.K., Black, J., Jasty, M., Galante, J.O., 1995. Local and distant products from modularity. Clin.l Ortho. Rel. Res. 319, 94–105.

Jauch, S.Y., Huber, G., Hoenig, E., Baxmann, M., Morlock, M.M., 2011. Influence of material coupling and assembly condition on the magnitude of micromotion at the stem-neck interface of a modular hip endoprosthesis. J. Biomechan. 44, 1747–1751.

Jauch, S.Y., Huber, G., Morlock, M.M., 2013. Micromotions at the taper interface between stem and neck adapter of a bimodular hip prosthesis during activities of daily living. J. Orthoped. Res. 31, 1165–1171.

Langton, D.J., Jameson, S.S., Joyce, T.J., Hallab, N.J., Natu, S., Nargol, A.V.F., 2010. Early failure of metal-on-metal bearings in hip resurfacing and large-diameter total hip replacement. J. Bone Joint Surg. 92B (1), 39–46.

Mali, S.A., Gilbert, J.L., 2016. Correlating Fretting Corrosion and Micromotions in Modular Tapers: Test Method Development and Assessment. In: Lemons, J., Mihalko, W. (Eds.), Greenwald, S. Amer Soc for Testing and Mat Special Technical Publication on Implant Modularity, pp. 471–480.

McCarthy, J.C., Bono, J.V., O'Donnell, P.J., 1997. Custom and modular components in primary total hip replacement. Clin. Orthoped. Relat. Res. 344, 162–171.

Ouellette, E.S., Shenoy, A.A., Gilbert, J.L., 2017. The seating mechanics of head-neck modular tapers in vitro: load-displacement measurements, moisture, and rate effects. J. Orthopaedic Res. 36 (4). https://doi.org/10.1002/jor.23725.

Pennock, A.T., Schmidt, A.H., Bourgeault, M., 2002. Morse-type tapers: factors that may influence taper strength during total hip arthroplasty. J. Arthroplasty 17 (6), 773–778.

Pierre, D., Gilbert, J.L., 2016. Effects of Seating Load Magnitude and Load Orientation on Seating Mechanics in Modular Taper Junctions. Transactions of the International Society of Arthroplasty, Boston MA.

Pierre, D., Gilbert, J.L., 2014. Incremental Cyclic Fretting Corrosion and Micromotion Test of Hip Implant Head-Neck Tapers. Transaction of the Society For Biomaterials. Denver CO..

Pierre, D., Swaminathan, V., Scholl, L.Y., TenHuisen, K., Gilbert, J.L., 2018. Effects of seating load magnitude on incremental cyclic fretting corrosion of 540' modular taper junctions. J. Arthroplasty 33 (6), 1953–1961.

Rehmer, A., Bishop, N.E., Morlock, M.M., 2012. Influence of assembly procedure and material combination on the strength of the taper connection at the head-neck junction of modular hip endoprosthesis. Clin. Biomechan. 27, 77–83.

Scholl, L., Pierre, D., Lee, R., Faizan, A., Swaminathan, V., TenHuisen, K., Gilbert, J.L., Nevelos, J., 2018. Effect of substrate compliance on total hip modular taper seating stability part H. J. Eng. Med. 232 (9), 862–870.